Article

Takagi–Sugeno Fuzzy Model-Based Control for Semi-Active Cab Suspension Equipped with an Electromagnetic Damper and an Air Spring

Bangji Zhang [1,2]**, Minyao Liu** [1]**, Kunjun Wang** [3]**, Bohuan Tan** [4]**, Yuanwang Deng** [1,*]**, An Qin** [1] **and Jingang Liu** [4]

[1] State Key Laboratory of Advanced Design and Manufacturing for Vehicle Body, Hunan University, Changsha 410082, China
[2] Intelligent Transportation System Research Center, Zhejiang University City College, Hangzhou 310015, China
[3] Bus Technical Department, CRRC Electric Vehicle Co., Ltd., Zhuzhou 412007, China
[4] School of Mechanical Engineering and Mechanics, Xiangtan University, Xiangtan 411105, China
* Correspondence: dengyuanwang610@126.com

Abstract: Variable damping shock absorbers have received extensive attention for their efficient vibration reduction performance, and air springs have also been widely used in high-end commercial vehicles due to their nonlinear stiffness characteristics. This paper presents a novel semi-active cab suspension integrated with an air spring and a variable damping electromagnetic damper (A-EMD). The electromagnetic damper (EMD) prototype was designed, manufactured and tested. Then, due to the interference of nonlinear stiffness characteristics of the air spring with the controller in the subsequent design, the Takagi–Sugeno fuzzy method was adopted to segmentally linearize its nonlinearity, based on which an H∞ state feedback semi-active controller was designed to control the EMD to generate variable damping force. Furthermore, a Luenberger state observer was designed to provide immeasurable state parameters for the controller. Numerical simulations were carried out to validate the effectiveness of the proposed approaches, and the results show that the proposed control strategy can significantly improve the ride comfort of the A-EMD system. The vibration dose value (VDV) acceleration under the bump road and the frequency-weighted acceleration root mean square (FWA-RMS) under the random road decreased by 36.05% and 19.77%, respectively, compared with the passive suspension system.

1. Introduction

Under the development and promotion of vehicle technology, commercial vehicles show the trends of being high-end, intelligent and having electronic control. In adapting to these three trends, improving the ride comfort of commercial vehicles is an important and urgent problem to be solved [1]. The cab suspension is between the frame and the cab, which can attenuate the vibration transmitted from the frame and give the driver a positive driving experience. Therefore, cab suspension is an effective way to improve the ride comfort of commercial vehicles [2].

According to the working principle of suspension, it can be divided into passive suspension, semi-active suspension and active suspension [3]. Passive suspension cannot always maintain adequate damping performance under variable road conditions due to its fixed stiffness and damping. Meanwhile, active suspension has the best damping performance, but it introduces active actuators, which require an external energy supply and high energy consumption, lacking in cost-effectiveness and practicality. Therefore, scholars are increasingly studying semi-active suspension. The performance of semi-active

suspension is similar to active suspension, but unlike the latter, semi-active suspension does not require additional devices and energy input, and its operating principle is mainly reflected in the controllable elastic elements and dampers [4]. The controllable elastic elements are mainly air springs, which have typical nonlinear stiffness characteristics and can be adjusted in stiffness by inflating and deflating the air spring. Although it can be controlled, there is hysteresis in gas control, which makes it difficult to achieve precise control, so only graded height adjustment is generally made [5]. Therefore, semi-active control is still mainly in the control of the dampers. Felix Weber et al. proposed a semi-active cable damper and proved its superior damping performance compared with a linear viscous damper. The influence of maximum and minimum damping coefficients of the semi-active cable damper on semi-active force tracking was also discussed [6]. However, one more thing to mention about air springs is that, compared to linear stiffness springs, air springs can improve ride comfort by relying only on their nonlinear stiffness characteristics even if they are not controlled, so they are still the preferred choice among suspension elastic elements. Furthermore, we also need to consider that the application of air springs requires us to deal with their nonlinear stiffness. Fortunately, the T-S fuzzy method is a convenient and effective way to deal with nonlinear systems [7], which has applications in wind power systems [8], stochastic network time delay processing [9] and so on.

The most studied controllable dampers in the field of suspension are continuous damping control (CDC) dampers, magnetorheological dampers and electromagnetic dampers, and many control algorithms have been designed to control them. The first to be introduced was the CDC damper, which was developed from the passive hydraulic damper with the addition of a high-precision solenoid valve to the former. Bilin et al. investigated a semi-active suspension system based on four CDC dampers for light commercial vehicles with coordinated upper and lower-level control. The four bottom layer controllers control each CDC damper using a hybrid control algorithm of the skyhook and groundhook. The upper layer controller then coordinates the four bottom layer controllers to keep the body attitude from excessive changes [10]. Qin's team designed five control algorithms, including improved skyhook control, hybrid control, and model-referenced sliding mode control, with CDC dampers as the object, and compared the degree of optimization of the control effect of each control algorithm [11]. In actually installed applications, Buick Grand Prix, Opel Astra and other high-end passenger car types as well as high-end commercial vehicle types such as Dongfeng Tianlong are equipped with CDC dampers. However, the current disadvantages of CDC dampers in terms of size, control accuracy, difficulty and response speed have not yet been adequately improved. Coinciding with the continuous development of magnetorheological technology, magnetorheological dampers were introduced, which can achieve the same size as oil pressure dampers, or even smaller, and their response speed is milliseconds. As a result, magnetorheological dampers have received a lot of attention and application. The core of the magnetorheological damper principle lies in its special magnetorheological fluid, which is a typically controlled fluid that can change from a free-flowing viscous fluid to a semi-solid under the action of a magnetic field, and its mechanical properties (damping) will increase or decrease with the change in magnetic field [12]. Magnetorheological dampers have been a major hot topic in the direction of semi-active suspensions, and scholars have designed various control algorithms to control them. Yao et al. used the skyhook semi-active control method for magnetorheological dampers in suspensions. Simulation and experimental results demonstrated the feasibility of magnetorheological dampers in semi-active vibration control of vehicle suspension systems [13]. Guo's team proposed a neural network control that includes an error back-propagation algorithm with a multilayer forward neural network quadratic momentum, and this algorithm can effectively handle the nonlinearity of magnetorheological dampers and has a greater advantage in controlling low-frequency vibrations [14]. Tang et al. also used a T-S fuzzy approach to segmentally linearize the nonlinearity brought about by magnetorheological dampers, and subsequently designed a state observer-based H∞ controller to control it, which was simulated and tested in a quarter-suspension system [15].

Moreover, magnetorheological dampers have been widely used in real vehicle suspensions, but their drawbacks are gradually exposed in practical terms, which are exactly what magnetorheological fluids bring: expensive, temperature-sensitive and with natural settling of fluid particles. In addition, it still does not solve the problem of control accuracy and difficulty. Because of these problems, the further promotion of magnetorheological dampers has been hampered and is still under continuous research. Just in recent years, the electromagnetic damper proposed by Ning's team entered the vision of scholars [16]. The electromagnetic damper consists of a generator with an external circuit, a linkage mechanism and a reduction mechanism. It has a compact structure and the components are standard parts, so the cost and size have obvious advantages over CDC dampers and magnetorheological dampers. In addition, the biggest advantage of this damper is that it does not need oil when it works, and only adjusts the output damping coefficient by changing the resistance value, and its damping force is linearly related to the current. Moreover, it also has advantages in energy consumption, response speed, control accuracy and difficulty. Ning used this electromagnetic damper on a seat suspension, and conducted experiments on a six-degree-of-freedom seat test rig using the H∞ control algorithm to verify its effective vibration damping performance.

Therefore, based on previous research and work, a new configuration of cab suspension based on an air spring and an electromagnetic damper (A-EMD) is proposed in this paper. The air spring is not controlled here, but improves the passive performance of the suspension system with its own exceptional nonlinear stiffness characteristics. Then, a Takagi–Sugeno fuzzy approach is used to deal with the nonlinearity brought by the air spring. As for the electromagnetic damper, a new structural form is designed according to the application scenario of the cab suspension, and then a state observer-based H∞ semi-active controller is designed to control it. The structure of this paper is as follows. In Section 2, the operating principle of A-EMD is introduced and mathematical modeling of A-EMD is carried out. Then, an EMD characteristic test is designed to verify the mathematical model of the EMD. Section 3 linearizes the A-EMD and designs the state observer-based H∞ semi-active controller accordingly. The simulation results are analyzed in Section 4.

2. Quarter-Cab Car Suspension with A-EMD

Air spring and electromagnetic damper are two important parts of A-EMD. Air spring has a typical nonlinear characteristic, which is shown in its nonlinear stiffness, varying with the change in its deformation variable. The characteristic of the electromagnetic damper is that its external circuit contains a variable resistance, which can make the damping of the electromagnetic damper change along with the varying resistance. Through this connection, the value of the resistance is related to the output damping force. In this section, a quarter-cab car suspension model containing A-EMD is developed, and the respective mathematical models of air spring and electromagnetic damper are derived based on their operating principles. Finally, the validity of the EMD mathematical model is also verified by a characteristic test of an EMD.

2.1. The Working Principle of A-EMD

The schematic diagram of A-EMD is shown in Figure 1, which consists of an air spring and an electromagnetic damper (generator with external circuit, ball screw mechanism, coupling and fixed bearing seat), where the three-phase generator and rectifier are simplified to a DC generator for the convenience of analysis. When the novel suspension system is excited by the outside disturbance, the A-EMD starts to vibrate up and down, and its vibration is absorbed by the air spring and electromagnetic damper, respectively. On the one hand, the air spring attenuates the amplitude to a certain extent due to its own nonlinear stiffness characteristics. On the other hand, the vibration of the suspension system is transformed into the rotational motion of the generator through the ball screw, and the output force of the damper is indirectly changed by varying the resistance of the

external circuit after the power supply of generator to external circuit. The control process is realized by the state observer-based H∞ control algorithm.

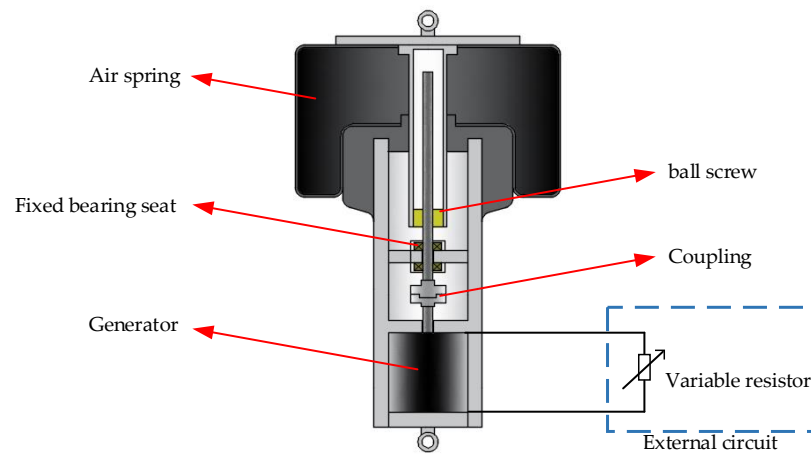**Figure 1.** The schematic diagram of A-EMD.

2.2. Quarter-Cab Car Suspension Model

The validation of the damping performance of A-EMD needs to rely on the dynamic response of the suspension system, so it is necessary to establish an effective suspension model [2]. To facilitate subsequent comparative verification of the controlled suspension and passive suspension performance, we construct here a quarter-cab car suspension comparison benchmark model, which can represent both the controlled and passive suspensions, respectively.

The specific structure diagram is shown in Figure 2. m_c, m_s and m_v are the cab mass, the sprung mass and the unsprung mass, respectively; k_c, k_s and k_t are the stiffness of the air spring, the stiffness of the car suspension and the tire stiffness, respectively; c_c, c_p and c_s are the controllable damping of the electromagnetic damper, the fixed damping of cab suspension and the damping of the car suspension, respectively; z_c, z_s and z_v are the displacements of the corresponding masses; z_r is the road displacement input.
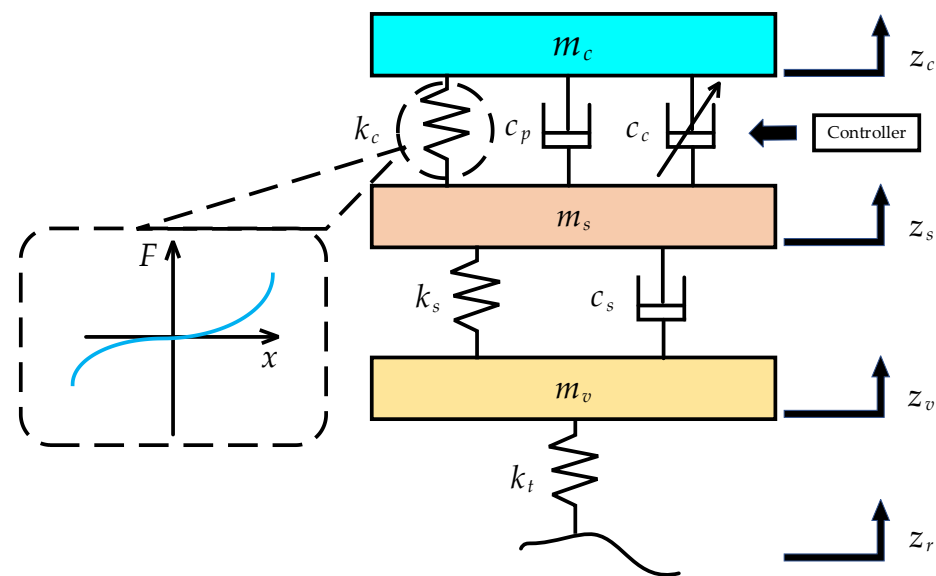

Figure 2. Quarter-cab car suspension benchmark model.

Suspension model parameter values are shown in Table 1, obtained from experimental measurements.

Table 1. Parameter values of the quarter-cab car suspension model.

Symbol	Value
m_c	794.5 kg
m_s	2364 kg
m_v	672 kg
k_s	492,400 N/m
k_t	1,728,000 N/m
c_p	2000 N·s/m
c_s	12,000 N·s/m

Note that if the controllable damping force is always zero, i.e., c_c is always zero, the suspension model is a passive model, at which point c_p is passive damping; otherwise, the model is a controllable model, c_p is zero and controllable damping force exists. Defining u as the controllable damping force of the electromagnetic damper, the kinetic equations of the model can be illustrated as follows:

$$\begin{cases} m_c\ddot{z}_c = -k_c(z_c - z_s) - c_p(\dot{z}_c - \dot{z}_s) - u \\ m_s\ddot{z}_s = -k_s(z_s - z_v) - c_s(\dot{z}_s - \dot{z}_v) + k_c(z_c - z_s) + c_p(\dot{z}_c - \dot{z}_s) + u \\ m_v\ddot{z}_v = -k_t(z_v - z_r) + k_s(z_s - z_v) + c_s(\dot{z}_s - \dot{z}_v) \end{cases} \quad (1)$$

To facilitate the design of subsequent observer and controller, Equation (1) is transformed into state–space form. The state variables and perturbation inputs are defined as:

$$x_1 = \dot{z}_c, \ x_2 = z_c - z_s, \ x_3 = \dot{z}_s, \ x_4 = z_s - z_v, \ x_5 = \dot{z}_v, \ x_6 = z_v - z_r, \ d = \dot{z}_r, \quad (2)$$

Then, the equation of state can be expressed as follows:

$$\dot{x} = Ax + B_u u + B_d d, \ x = [x_1 \ x_2 \ x_3 \ x_4 \ x_5 \ x_6]^T,$$

$$A = \begin{bmatrix} -\frac{c_p}{m_c} & -\frac{k_c}{m_c} & \frac{c_p}{m_c} & 0 & 0 & 0 \\ 1 & 0 & -1 & 0 & 0 & 0 \\ \frac{c_p}{m_s} & \frac{k_c}{m_s} & -\frac{c_p+c_s}{m_s} & -\frac{k_s}{m_s} & \frac{c_s}{m_s} & 0 \\ 0 & 0 & 1 & 0 & -1 & 0 \\ 0 & 0 & \frac{c_s}{m_v} & \frac{k_s}{m_v} & -\frac{c_s}{m_v} & -\frac{k_t}{m_v} \\ 0 & 0 & 0 & 0 & 1 & 0 \end{bmatrix}, \ B_u = \begin{bmatrix} -\frac{1}{m_c} \\ 0 \\ \frac{1}{m_s} \\ 0 \\ 0 \\ 0 \end{bmatrix}, \ B_d = \begin{bmatrix} 0 \\ 0 \\ 0 \\ 0 \\ 0 \\ -1 \end{bmatrix} \quad (3)$$

2.3. Mathematical Model of Air Spring

Since the properties of air springs are complex, involving thermodynamics, dynamics and aerodynamics, it is practical to make several assumptions before proceeding to the following derivation:

- The gas inside the airbag is regarded as ideal gas;
- The process of gas state change in the air spring is regarded as a quasi-static process;
- The air spring is not charged or deflated, but has an initial pressure P_0 and an initial volume V_0.
- The simplified physical model of the air spring is shown in Figure 3. We can infer from Figure 3 that air spring can only withstand vertical forces. When it is subjected to vertical pressure, it will produce a vertical reaction force, which is defined as follows:

$$F_{air} = (P - P_a)A_e,\tag{4}$$

where P is the absolute pressure in the air spring at this moment; P_a is the atmospheric pressure; A_e is the effective area of the air spring. Notice that A_e is not a specific geometric area, which is usually obtained by constant pressure static load test of the air spring, and it is always the function of the air spring deformation variable. Here, based on the work of Wang Dong at Hunan University [17], the effective area relationship formula is given:

$$A_e = -531\Delta h^5 - 4.68\Delta h^4 + 10.6\Delta h^3 - 0.601\Delta h^2 + 0.00261\Delta h + 0.0451,\tag{5}$$
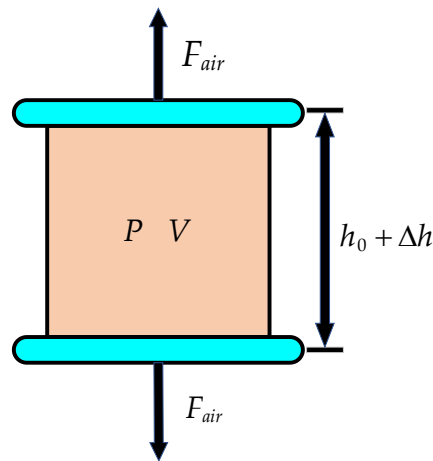
where Δh is the air spring deformation variable.

Figure 3. The simplified physical model of the air spring.

Next, considering that the dynamic vibration process of the air spring is actually a multivariable process, the multivariable equation for the ideal gas can be obtained in exactly the same equation form as the adiabatic equation. In addition, given that the air spring is deformed under the load, the internal volume and pressure of its airbag are always changing, so the ideal gas multivariable equation can be expressed as:

$$PV^n = P_0 V_0^n = const,\tag{6}$$

where V is the volume of the air spring at this moment and n is a multivariate exponent. Thereinto, V satisfies the following relation:

$$V = (h_0 - \Delta h)A_e,\tag{7}$$

where h_0 is the initial height of the air spring.

Combining Equations (4)–(7), the force of the air spring at any time can be illustrated as follows:

$$F_{air} = \left(\frac{P_0 V_0^n}{[A_e(h_0 - \Delta h)]^n} - P_a\right)A_e,\tag{8}$$

The stiffness of the air spring can be obtained by taking the derivative of the elastic force with respect to the deformation variable:

$$k = \frac{dF_{air}}{d(\Delta h)} = P_0 V_0^n \frac{kA_e^2 - (k-1)(h_0 - \Delta h)A_e \frac{dA_e}{d(\Delta h)}}{[A_e(h_0 - \Delta h)]^{n+1}} - P_a \frac{dA_e}{d(\Delta h)},\tag{9}$$

The parameter values of the air spring are given in Table 2 [17]. The mechanical behaviors of the air spring are shown in Figure 4. We can see from Figure 4 that the stiffness of the air spring demonstrates the basic characteristics of low deformation with low stiffness and high deformation with high stiffness, and this variation is nonlinear. Meanwhile, the elastic force of the air spring can be seen to be steep at large deformations and flat at small deformations, which means that it can effectively reduce vibration under rough road conditions and ensure better comfort on gentle roads.

Table 2. Parameter values of the air spring.

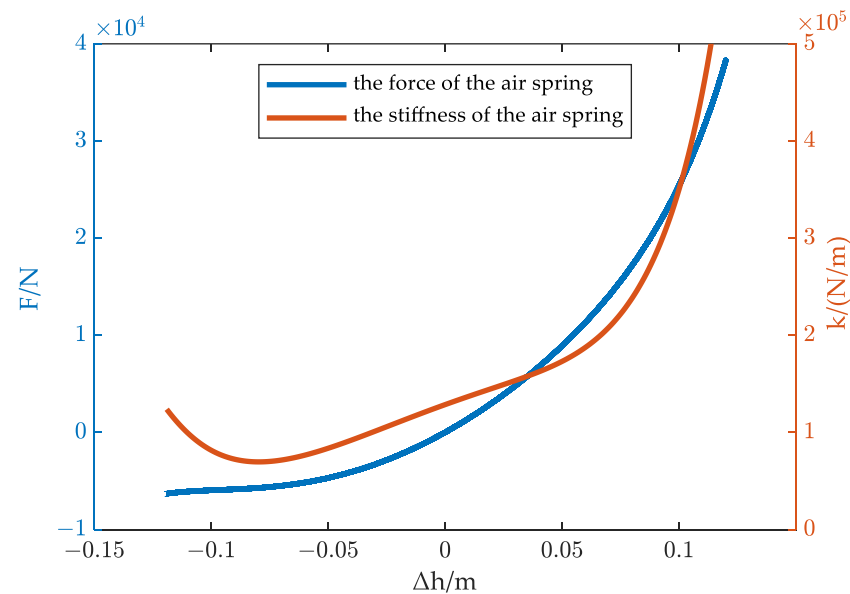| Symbol	Value
P_0	0.7 MPa
V_0	9.5 L
h_0	0.252 m
P_a	0.1 MPa
n	1.381

Figure 4. The mechanical behavior of air spring.

2.4. Mathematical Model of Electromagnetic Damper

The electromagnetic damper consists of two parts, the main structure (generally includes the generator and ball screw) and the external circuit. Figure 5 is the energy flow of the electromagnetic damper. Based on Figure 5, a mathematical model of the electromagnetic damper is established.
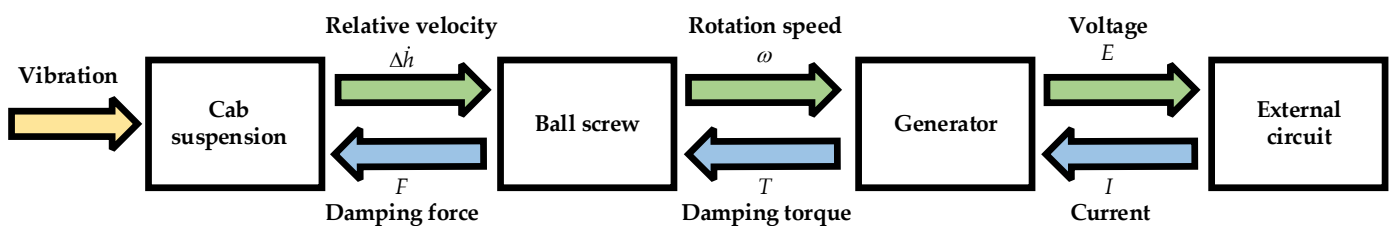

Figure 5. The energy flow of electromagnetic damper.

Firstly, the suspension moves up and down when it receives the excitation of external disturbance, and then the linear motion is converted into rotary motion by the ball screw and transmitted to the generator, whose rotation speed relationship is expressed as follows:

$$\omega = r_b \Delta \dot{h}, \tag{10}$$

where r_b is the transmission ratio of the ball screw contained in the electromagnetic damper.

The generator accordingly generates an electric potential during the rotation, which energizes the external circuit. The generated voltage E and the circuit current I are as follows:

$$E = k_e \omega, \tag{11}$$

$$I = \frac{E}{(R_m + \widetilde{R})}, \tag{12}$$

where k_e is the voltage constant; R_m is the internal resistance of the generator; $\widetilde{R}$ is the variable resistance, which varies within a range $[0, R_{\max}]$. $R_{\max}$ is the maximum value of the variable resistance.

Then the current I will cause the generator to generate a damping torque T:

$$T = k_i I, \tag{13}$$

Where k_i is the torque constant and generators generally have $k_i = k_e$.

Combining Equations (10)–(13), the damping torque is transformed into a damping force F through the ball screw:

$$F = r_b T = \frac{k_i k_e r_b^2}{R_m + \widetilde{R}} \Delta \dot{h}, \tag{14}$$

Finally, the variable damping of the electromagnetic damper is

$$c_c = \frac{k_i k_e r_b^2}{R_m + \widetilde{R}}, \tag{15}$$

The parameter values of the electromagnetic damper are shown in Table 3, obtained from parameter identification experiments.

Table 3. Parameter values of the electromagnetic damper.

| Symbol	Value
k_i	0.454 N·m/A
k_e	0.454 V·s/rad
r_b	628.3
R_m	7.625 Ω
$R_{\max}$	120 Ω

2.5. The Characteristic Experiment for the Electromagnetic Damper

In order to verify the accuracy of the mathematical model of the electromagnetic damper, a prototype was trial-produced and the damping characteristic was tested on an MTS (the world's largest supplier of mechanical property testing and simulation systems) test stand. The mechanical part of the electromagnetic damper is modeled as shown in Figure 6. It contains a ball screw mechanism with a lead of 16 mm, a fixed bearing housing, a coupling, a 400 W generator, protective housing and other connection parts.
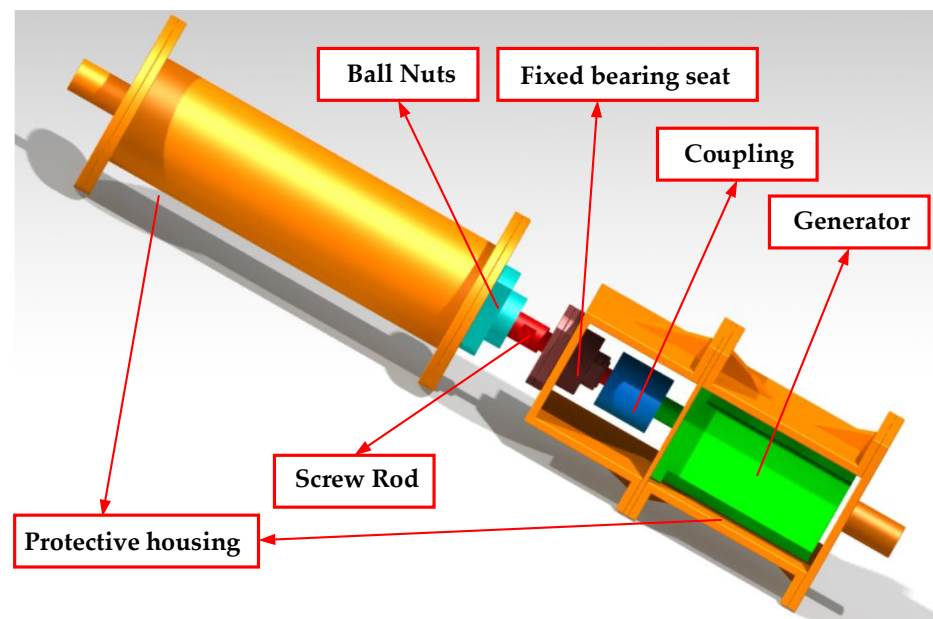
Figure 6. The prototype model of the electromagnetic damper.

The test system is shown in Figure 7. When the MTS test stand pulls the electromagnetic damper up and down in the form of a sinusoidal excitation, the generator first converts the three-phase AC power to DC power through a rectifier and connects to the external circuit. Then, the circuit current is varied by changing the resistance in the circuit, which changes the damping force of the electromagnetic damper. Finally, the damping force is measured by the force sensors.
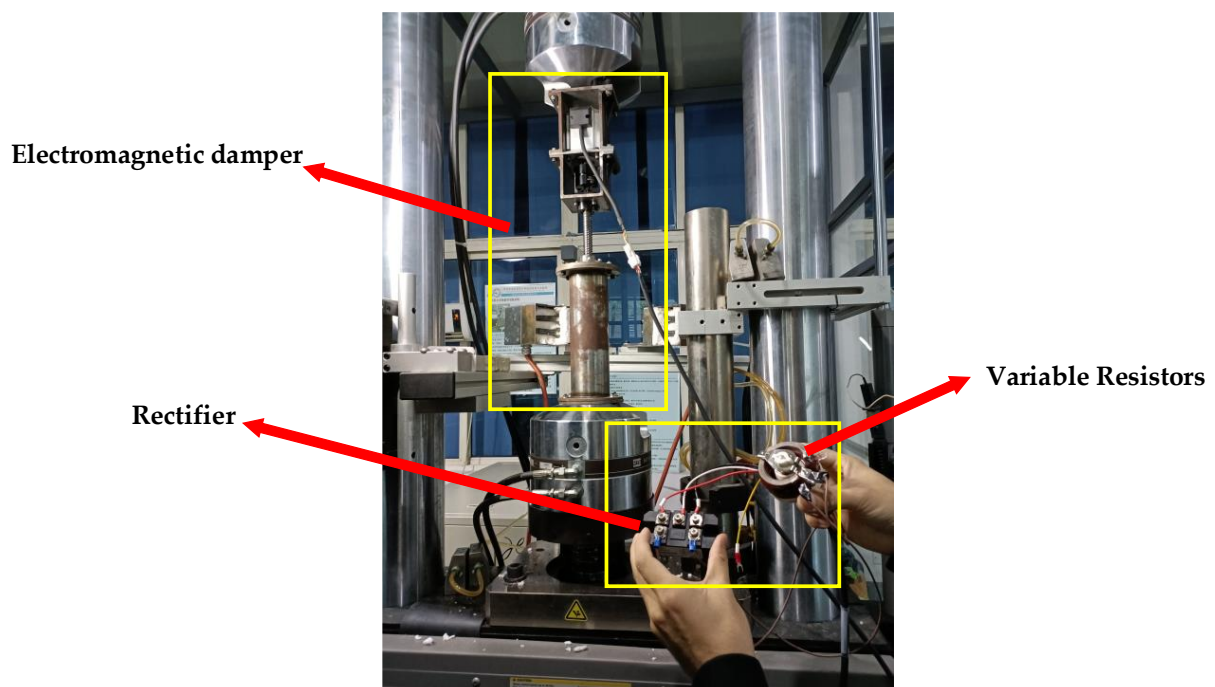
Figure 7. Experimental system with MTS.

The experiment of variable resistance was as follows. According to the real motion state of the cab suspension, the loading frequency and working amplitude of the MTS were set to 1 Hz and ±40 mm, respectively. According to the damping force range required for cab suspension, the external resistance of the electromagnetic damper was set to 2, 10

and 40 ohm. Then, we tested the damping force of the electromagnetic damper when the resistance value changed. The mathematical model derived above was simulated by the Simulink platform under the same excitation conditions and parameters. The simulation results and the experimental results are illustrated in Figure 8.
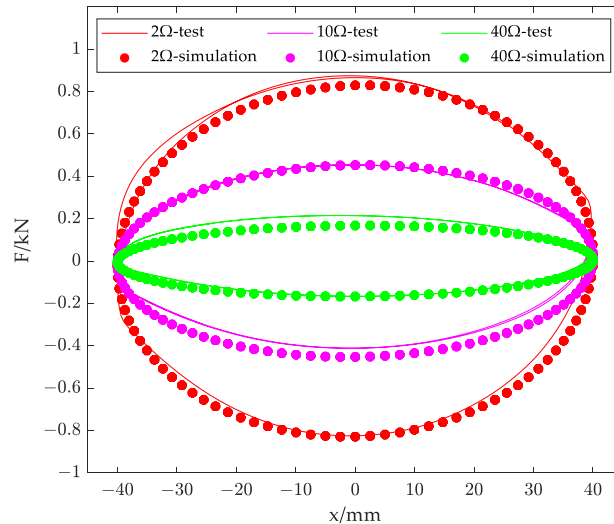

Figure 8. Test and simulation damping characteristics response results.

It can be seen from Figure 8 that the experimental results and simulation results almost match. This indicates that the mathematical model derived above can effectively represent the electromagnetic damper.

3. Semi-Active Control Strategy for T-S Fuzzy Suspension Model

The T-S fuzzy method was used to deal with the nonlinearity of the air spring. Afterwards, for the segmented linear model, the design of the state observer and the semi-active controller was carried out according to the principle of parallel distributed compensation (PDC). The process of control and observation is shown in Figure 9.
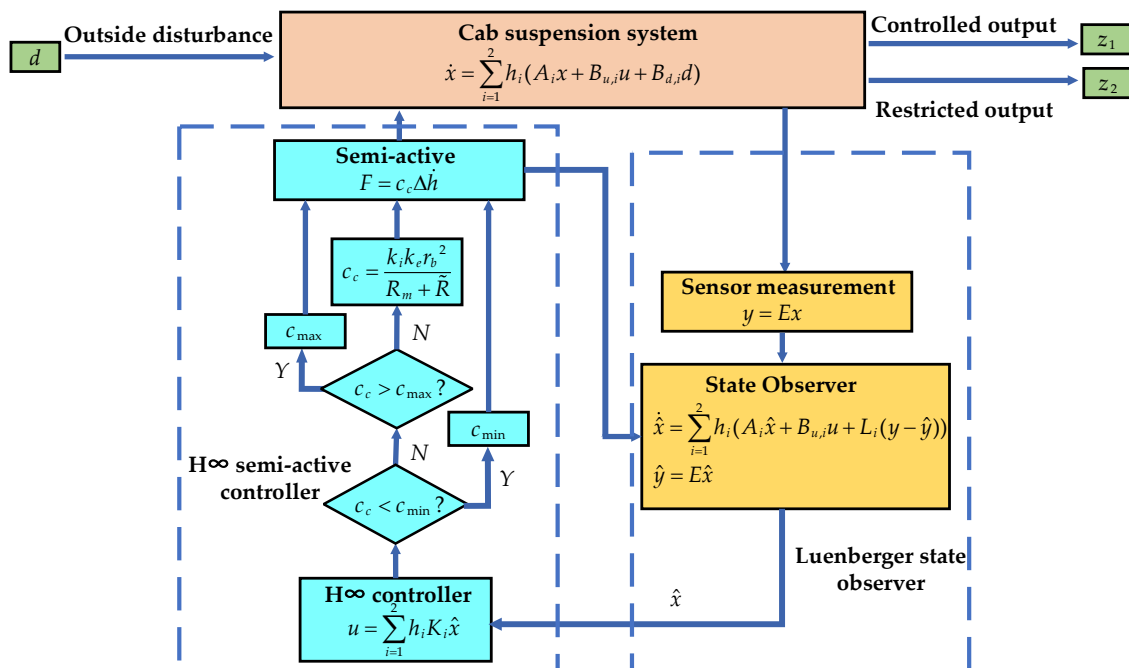

Figure 9. The process of control and observation.

3.1. T-S Fuzzy Model of Suspension System

The nonlinear stiffness of the air spring k_c causes the suspension system to be nonlinear, and direct control of the nonlinear system can be complicated. Considering that this stiffness is bounded in practice, the original nonlinear system can be reasonably represented by linear subsystems using the T-S fuzzy approach. The representation of the stiffness is as follows:

$$k_c = h_1 \underline{k}_c + h_2 \overline{k}_c,\tag{16}$$

$$h_1 = \frac{\overline{k}_c - k_c}{\overline{k}_c - \underline{k}_c}, h_2 = \frac{k_c - \underline{k}_c}{\overline{k}_c - \underline{k}_c},\tag{17}$$

where h_1 and h_2 are fuzzy membership functions, and $h_1 + h_2 = 1$; $\overline{k}_c$ and $\underline{k}_c$ represent the upper and lower boundaries of the stiffness of the air spring, respectively.

The original model is then divided into two linear models:

$$\begin{aligned} IF\ k_c = \underline{k}_c\ THEN\ \dot{x}_1 = A_1 x + B_{u,1} u + B_{d,1} d, \\ IF\ k_c = \overline{k}_c\ THEN\ \dot{x}_2 = A_2 x + B_{u,2} u + B_{d,2} d' \end{aligned}\tag{18}$$

Thus, the T-S fuzzy model for the suspension system is obtained as:

$$\dot{x} = \sum_{i=1}^{2} h_i (A_i x + B_{u,i} u + B_{d,i} d),\tag{19}$$

where A_i, $B_{u,i}$ and $B_{d,i}$ are matrixes that replaces k_c with $\overline{k}_c$ or $\underline{k}_c$. For brevity of subsequent observer and controller derivation, $\sum_{i=1}^{2} h_i A_i$, $\sum_{i=1}^{2} h_i B_{u,i}$ and $\sum_{i=1}^{2} h_i B_{d,i}$ are defined as A_h, $B_{u,h}$ and $B_{d,h}$, respectively.

3.2. Luenberger State Observer Design

The design of the state feedback controller needs to be based on the state of the system, but not all state parameters can be directly measured by sensors in the actual process. A common approach is to design a state observer that uses measurable parameters to observe other parameters that cannot be measured. As the dynamic deflections and the relative velocities can be measured directly, the measurement equation is expressed as:

$$y = Ex,\ y = \begin{bmatrix} z_c - z_s & z_s - z_v & \dot{z}_c - \dot{z}_s & \dot{z}_s - \dot{z}_v \end{bmatrix},$$
$$E = \begin{bmatrix} 0 & 1 & 0 & 0 & 0 & 0 \\ 0 & 0 & 0 & 1 & 0 & 0 \\ 1 & 0 & -1 & 0 & 0 & 0 \\ 0 & 0 & 1 & 0 & -1 & 0 \end{bmatrix}\tag{20}$$

Then, the Luenberger state observer can be designed as:

$$\dot{\hat{x}} = A_h \hat{x} + B_{u,h} u + L_h (y - \hat{y}),\tag{21}$$

where $\hat{y} = E\hat{x}$; $L_h = \sum_{i=2}^{2} h_i L_i$ is the observer matrices gain to be designed.

The main goal of the observer design is that the observed state is as close to the real state as possible, so the estimation error is defined as:

$$e = x - \hat{x},\tag{22}$$

According to Equations (19) and (21), and then deriving for Equation (22), we can obtain the dynamic equation of the state estimation error:

$$\dot{e} = \dot{x} - \dot{\hat{x}} = (A_h - L_h E)e + B_{d,h}d, \tag{23}$$

The next step is the design of the controller.

3.3. Robust H∞ Controller Design Based on State Observer

Considering H∞ control has strong robust performance, the H∞ control algorithm is popular in vehicle suspension control [18]. Therefore, the H∞ control algorithm is also used in this paper. The observer-based H∞ state feedback controller can be represented as:

$$u = K_h \hat{x}, \tag{24}$$

where $K_h = \sum\limits_{i=2}^{2} h_i K_i$ is the state feedback gain matrices to be designed.

Ride comfort, road holding ability and suspension deflection are three main performance criteria in suspension design, and ride comfort is of the greatest concern, which can be quantified by the cab acceleration. Therefore, the state space of the control output is represented as follows:

$$z_1 = Cx + D_u u, \ z_1 = \ddot{z}_c,$$
$$C = \left[-\frac{c_p}{m_c} \ -\frac{k_c}{m_c} \ \frac{c_p}{m_c} \ 0 \ 0 \ 0 \right]^T, \ D_u = -\frac{1}{m_c} \tag{25}$$

In conjunction with the T-S fuzzy model in this paper, control output can be also rewritten as:

$$z_1 = C_h x + D_{u,h} u, \tag{26}$$

where $C_h = \sum\limits_{i=1}^{2} h_i C_i$ and $D_{u,h} = \sum\limits_{i=1}^{2} h_i D_{u,i}$.

However, there is a contradiction between the three performance criteria of the suspension, when considering that only the ride comfort will always sacrifice the suspension deflection and road holding ability, so the other two indicators of the suspension are restricted output to ensure that the vehicle is in a relatively compromised state. The following constraints should be satisfied [19]:

$$|z_c - z_s| \leq z_{\max 1}, \tag{27}$$

$$|z_s - z_v| \leq z_{\max 2}, \tag{28}$$

$$|k_t(z_v - z_r)| \leq (m_c + m_s + m_v)g, \tag{29}$$

where $z_{\max 1}$ and $z_{\max 2}$ are the restricted travel of the cab suspension and the car suspension, respectively; g is gravitational constant (9.8 N/kg). $z_{\max 1} = 0.1$ m and $z_{\max 2} = 0.15$ m are chosen here [20].

Based on the above inequality, the state space representation of the restricted output can be obtained:

$$z_2 = C_c x, \ z_2 = \left[\frac{(z_c - z_s)}{z_{\max 1}} \quad \frac{(z_s - z_v)}{z_{\max 2}} \quad \frac{k_t(z_v - z_r)}{(m_c + m_s + m_v)g} \right]^T,$$
$$C_c = \begin{bmatrix} 0 & \frac{1}{z_{\max 1}} & 0 & 0 & 0 & 0 \\ 0 & 0 & 0 & \frac{1}{z_{\max 2}} & 0 & 0 \\ 0 & 0 & 0 & 0 & 0 & \frac{k_t}{(m_c + m_s + m_v)g} \end{bmatrix} \tag{30}$$

Since the joint solution of the state observer and the state feedback controller is to be performed, the suspension system and the error system are to be combined, i.e., the observation error system and the suspension system are to be expanded into a more generalized system. Before that, the expressions of the relationship between the states of the two systems need to be obtained. Substitute Equations (23) and (24) into Equation (19), then

$$\dot{x} = (A_h + B_{u,h}K_h)x - B_{u,h}K_h e + B_{d,h}d, \tag{31}$$

Combining Equations (23) and (31) yields:

$$\dot{\overline{x}} = \overline{A}\overline{x} + \overline{B}d, \tag{32}$$

$$z_1 = \overline{C}\overline{x}, \tag{33}$$

where

$$\overline{x} = \begin{bmatrix} x \\ e \end{bmatrix}, \overline{A} = \begin{bmatrix} A_h + B_{u,h}K_h & -B_{u,h}K_h \\ 0 & A_h - L_h E \end{bmatrix}, \overline{B} = \begin{bmatrix} B_{d,h} \\ B_{d,h} \end{bmatrix}, \overline{C} = \begin{bmatrix} C_h + D_{u,h}K_h & -D_{u,h}K_h \end{bmatrix}$$

In order to make the controller have better performance under different vibration conditions, H∞ performance index is selected as:

$$\| T_{zd} \|_\infty = \sup \frac{\| z_1 \|_2}{\| d \|_2} (\| d \|_2 \neq 0), \tag{34}$$

where $\| z_1 \|_2 = \int_0^\infty z_1{}^T(t)z_1(t)dt$ and $\| d \|_2 = \int_0^\infty d^T(t)d(t)dt$.

Selecting the Lyapunov function for the system (32) as:

$$V(\overline{x}) = \overline{x}^T P \overline{x}, \tag{35}$$

where P is a positive definite symmetric matrix and $P = \begin{bmatrix} P_1 & 0 \\ 0 & P_2 \end{bmatrix}$.

By differentiating Equation (35) and using Equation (32), we obtain:

$$\dot{V}(\overline{x}) = (\overline{A}\overline{x} + \overline{B}d)^T P \overline{x} + \overline{x}^T P(\overline{A}\overline{x} + \overline{B}d), \tag{36}$$

Adding $z_1{}^T z_1 - \gamma^2 d^T d$ ($\gamma > 0$) to the two sides of Equation (36), which represents the performance index shown in Equation (34), we obtain:

$$\dot{V}(\overline{x}) + z_1{}^T z_1 - \gamma^2 d^T d = \begin{bmatrix} \overline{x} \\ d \end{bmatrix}^T \begin{bmatrix} \overline{A}^T P + P\overline{A} + \overline{C}^T\overline{C} & * \\ \overline{B}^T P & -\gamma^2 \end{bmatrix} \begin{bmatrix} \overline{x} \\ d \end{bmatrix}, \tag{37}$$

where * is used to represent a term that is induced by symmetry, and γ is a performance index.

Based on Equation (37), we make a definition:

$$\Theta = \begin{bmatrix} \overline{A}^T P + P\overline{A} + \overline{C}^T\overline{C} & * \\ \overline{B}^T P & -\gamma^2 \end{bmatrix}, \tag{38}$$

It can be deduced that if $\Theta < 0$, then $\dot{V}(x) + z_1{}^T z_1 - \gamma^2 d^T d < 0$ and $\| T_{zd} \|_\infty < \gamma$ with the initial condition $\overline{x}(0) = 0$. By applying the Schur's complement theorem, $\Theta < 0$ is equivalent to

$$\Xi = \begin{bmatrix} \overline{A}^T P + P\overline{A} & * & * \\ \overline{B}^T P & -\gamma^2 & * \\ \overline{C} & 0 & -I \end{bmatrix} < 0, \tag{39}$$

where I represents the identity matrix.

By pre-multiplying and post-multiplying Equation (39) with $diag\begin{bmatrix} P_1^{-1} & I & I & I \end{bmatrix}$, replacing $\overline{A}$, $\overline{B}$ and $\overline{C}$ in Equation (39), and doing the following transformation: $Q = P_1^{-1}$, $R_h = K_h Q$ and $G_h = P_2 L_h$, we will get the matrix:

$$\Xi = \begin{bmatrix} * + A_h Q + B_{u,h} R_h & * & * & * \\ -K_h^T B_{u,h}^T & * + P_2 A_h - G_h E & * & * \\ B_{d,h}^T & B_{d,h}^T P_2 & -\gamma^2 & * \\ C_h Q + D_{u,h} R_h & -D_{u,h} K_h & 0 & -I \end{bmatrix} < 0, \tag{40}$$

Because the observer-based control problem is not a simple LMI problem, P_1, P_2, K_h and L_h cannot be solved at the same time. Thus, this paper uses the two-step method [21] to solve the problem.

In addition, the restrict output should also be considered, whose performance index can be expressed as follows:

$$\| z_2 \|_\infty = \gamma \| d \|_2, \tag{41}$$

where $\| z_2 \|_\infty = \sup_{t \in [0,\infty)} \sqrt{z_2^T(t) z_2(t)}$.

If Equation (41) is satisfied, then the following formula is given [19]:

$$C_c^T C_c < P_1, \tag{42}$$

By using the Schur complement, Equation (42) can be rewritten as:

$$\begin{bmatrix} P_1 & * \\ Cc & I \end{bmatrix} > 0, \tag{43}$$

Pre-multiplying and post-multiplying with $diag\begin{bmatrix} P_1^{-1} & I \end{bmatrix}$ and performing the transformation $Q = P_1^{-1}$, Equation (43) is equivalent to

$$\begin{bmatrix} Q & * \\ CcQ & I \end{bmatrix} > 0, \tag{44}$$

To sum up, solving Equations (40) and (44), the observer gain and the controller gain can be obtained. However, it is worth noting that since the suspension system in this paper is a T-S fuzzy system, the final solution results also depend on the mechanical performance of the air spring under specific external disturbances, i.e., the maximum and minimum stiffness values, which also affect the establishment of the fuzzy rules. Therefore, there are observer gains and controller gains for each type of external disturbance in the suspension system. The specific solution results are given in the subsequent road excitation modeling.

Now, the desired active control force is obtained and the desired damping of the electromagnetic damper is expressed as follows:

$$c_c = \begin{cases} -\dfrac{u}{\dot{x}_2} & (\dot{x}_2 \neq 0) \\ c_{\max} & (\dot{x}_2 = 0) \end{cases}, \tag{45}$$

where $c_{\max}$ is the maximum damping of the electromagnetic damper. The damper can not generate damping force when $\dot{x}_2 \neq 0$, thus c_c can be any value in this moment. In this case it is assigned $c_{\max}$ for security.

And the damping of electromagnetic dampers can only vary between the maximum $c_{\max}$ and minimum damping $c_{\min}$ because of the limitations of their own structure, which are expressed as follows:

$$c_{\max} = \frac{k_i k_e r_b^2}{R_m}, \tag{46}$$

$$c_{\min} = \frac{k_i k_e r_b^2}{R_m + R_{\max}}, \tag{47}$$

$c_c < c_{\min}$ and $c_c > c_{\max}$ means that the required force can only be generated by the active actuator, the electromagnetic damper can not meet the requirement. Therefore, we can assign $c_c = c_{\min}$ when $c_c < c_{\min}$ and $c_c = c_{\max}$ when $c_c > c_{\max}$.

4. Numerical Simulations

In this section, the proposed controller is evaluated by comparing it with the passive suspension. To verify the transient and steady-state response of the controller proposed in this paper, two typical road excitations, i.e., bump road disturbance and random road disturbance, are applied.

4.1. Road Input Excitation Model

The first type of typical road is random road excitation, which is usually used to evaluate the vibration damping performance of suspension. It can be described by the following equation [22]:

$$\dot{z}_r(t) = -2\pi n_{00} v_0 \dot{z}_r(t) + 2\pi n_0 \sqrt{G_q(n_0) v_0} \omega(t), \tag{48}$$

where n_{00} and n_0 are cut-off frequency of road space and standard spatial frequency, respectively; the value of n_{00} and n_0 are normally chosen as 0.01 m^{-1} and 0.1 m^{-1}. v_0 is the vehicle forward velocity, which is chosen as 9.5 km/h. $G_q(n_0)$ is geometric mean of pavement grade and $\omega(t)$ is white noise. Here, we select grade D road surface, which can be represented by $G_q(n_0) = 1024 \times 10^{-6} \text{ m}^3$.

Another road is bump road, which is often applied to describe the impact resistance of suspension, which is given by [23]:

$$z_r(t) = \begin{cases} \frac{h_b}{2}(1 - \cos(\frac{2\pi v_0}{l} t)) & ,0 \leq t \leq \frac{l}{v_0} \\ 0 & ,t > \frac{l}{v_0} \end{cases}, \tag{49}$$

where h_b and l are the height and length of the bump, respectively. Here, $h_b = 0.05$ m and $l = 0.8$ m are chosen based on actual measurements. Again, the vehicle forward velocity v_0 is still set as 9.5 km/h.

Then, based on the cab suspension deflections range of the passive suspension under different road conditions, the maximum and minimum stiffness values of the air spring at this time can be derived, so that the linear system can be determined. The results of the controller and observer solutions are as follows.

For random road excitation, the solution results are:

$$K_1 = \begin{bmatrix} 2225.0181 & 67586.2278 & -3176.9630 & 68253.0741 & -194.5387 & 87947.9885 \end{bmatrix},$$

$$K_2 = \begin{bmatrix} 2075.8508 & -23482.5342 & -1391.6949 & 64060.8221 & 41.1195 & 87595.4783 \end{bmatrix},$$

$$L_1 = \begin{bmatrix} -35.4520 & -115.0538 & 54.8302 & 0.3549 \\ 1.5580 & 4.4086 & -1.8838 & -0.0763 \\ -40.4707 & -141.0501 & -59.2134 & -7.8611 \\ 1.5322 & 5.2678 & 2.2698 & 1.7381 \\ -288.6256 & -1052.3618 & -845.0339 & -3193.9499 \\ 92.5592 & 331.9484 & 304.9241 & 1229.5779 \end{bmatrix},$$

$$L_2 = \begin{bmatrix} -134.7522 & -115.3956 & 57.3913 & 0.2098 \\ 5.0871 & 4.4149 & -2.1296 & -0.0455 \\ -40.4707 & -140.3726 & -60.5488 & -7.8876 \\ 5.2691 & 5.2412 & 2.3030 & 1.7420 \\ -991.2153 & -1039.7321 & -879.7403 & -3195.4031 \\ 305.3366 & 327.0390 & 316.3469 & 1228.6055 \end{bmatrix},$$

For bump road excitation, the solution results are:

$$K_1 = \begin{bmatrix} 3636.1771 & 180086.2037 & -5406.0345 & 85511.0562 & -468.8914 & 104574.5532 \end{bmatrix},$$

$$K_2 = \begin{bmatrix} 3194.4751 & -9902.6076 & -2955.5604 & 79459.2876 & -69.2890 & 109894.1395 \end{bmatrix},$$

$$L_1 = \begin{bmatrix} -5.6494 & -74.0871 & 2.0321 & 6.0089 \\ 0.6438 & 0.3307 & -1.7711 & -6.9070 \\ -2.7910 & -140.7901 & 0.4041 & 2.1989 \\ 0.1326 & 0.5564 & 10.9425 & -19.8153 \\ -18.6322 & -650.1836 & -46.6086 & -57.7897 \\ 30.4630 & 11.3509 & 762.3921 & 4272.8694 \end{bmatrix},$$

$$L_2 = \begin{bmatrix} -172.0104 & -74.1029 & 2.1885 & 6.0134 \\ 0.2798 & 0.1819 & -30.0540 & -7.6813 \\ -28.6532 & -140.7819 & 0.5065 & 2.2014 \\ 0.0334 & 0.5250 & 10.8032 & -19.8184 \\ -163.4682 & -649.8963 & -46.3823 & -57.7847 \\ -29.4990 & 2.8245 & 767.7734 & 4273.0039 \end{bmatrix}.$$

4.2. Performance Verification of the Novel Suspension −

The main evaluation index of the suspension performance is the cab acceleration, while the dynamic deflection of the suspensions and the tire dynamic load are auxiliary indexes, i.e., the goal is to keep the cab acceleration low without exceeding the limit of the auxiliary indexes. Generally, random road excitation response is measured by RMS value and bump road excitation response is measured by peak-to-peak (PTP) value. To better quantify the improvement of ride comfort from a human perspective, the international standard ISO-2631-1 is also used for additional evaluation of cab acceleration in this paper. Combining the international standard and two typical road application scenarios, the frequency-weighted RMS (FW-RMS) acceleration and the fourth power vibration dose value (VDV) acceleration are used to evaluate the cab acceleration response under random road and bump road, respectively, which are expressed as Equations (50) and (51). The evaluation process is shown in Figure 10.
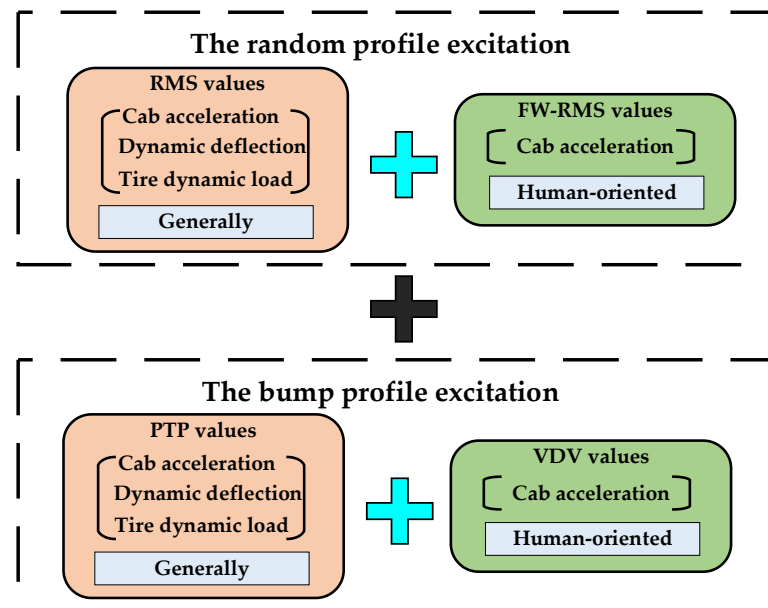

Figure 10. The evaluation process.

$$a_{FW-RMS} = \left[\frac{1}{T}\int_0^T \left\{a_{FW-RMS}(t)^2 dt\right\}\right]^{\frac{1}{2}}, \tag{50}$$

$$VDV = \left[\int_0^T \left\{a_w(t)^4 dt\right\}\right]^{\frac{1}{4}} \tag{51}$$

Then, based on the previously established T-S fuzzy suspension system and the designed controller, simulations were performed on the MATLAB/Simulink platform. The time domain responses of the two suspension systems for random road surfaces are compared in Figure 11, and the RMS values are shown in Table 4.
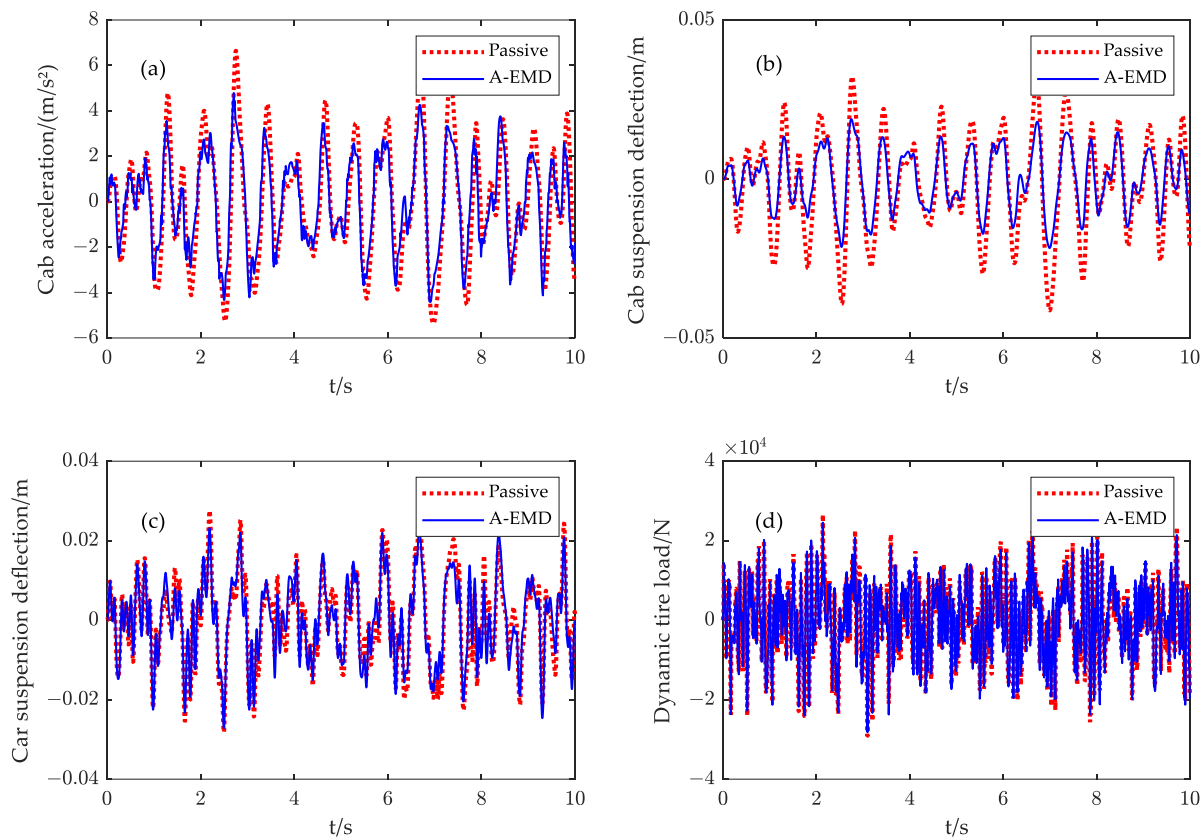
Figure 11. Response under random road excitation: (**a**) cab acceleration; (**b**) cab suspension deflection; (**c**) car suspension deflection; (**d**) dynamic tire load.

Table 4. RMS values.

Object	Passive	A-EMD
Cab acceleration (m/s²)	2.5399	2.0207
%	−	−20.44
Cab suspension deflection (m)	0.0153	0.0092
%	−	−39.82
Car suspension deflection (m)	0.0106	0.0100
%	−	−5.97
Tire dynamic load (N)	9097.8	8889.1
%	−	−2.29

Given the structural limitations of the electromagnetic damper, the semi-active force cannot always follow the active force, which is shown in Figure 12. Because the damping force is proportional to the relative speed of the suspension, the electromagnetic damper cannot output the opposite force when the ideal active force and relative speed are in opposite directions. Thus, the enhancement effect is limited. However, based on the structural limitations, it also can be seen from Figure 11a and Table 4 that the A-EMD still reduces the level of cab acceleration (−20.44%) compared with passive one. In addition, other suspension criteria, i.e., the restricted outputs, do not exceed their limit, and even their values have been reduced to varying degrees, which are shown in Figure 11b–d. Furthermore, we can also infer from Figure 13 that the FW-RMS acceleration decreases by 19.77%, which means that the A-EMD can also adapt well to the human-sensitive droop frequency band and effectively enhance passenger comfort.
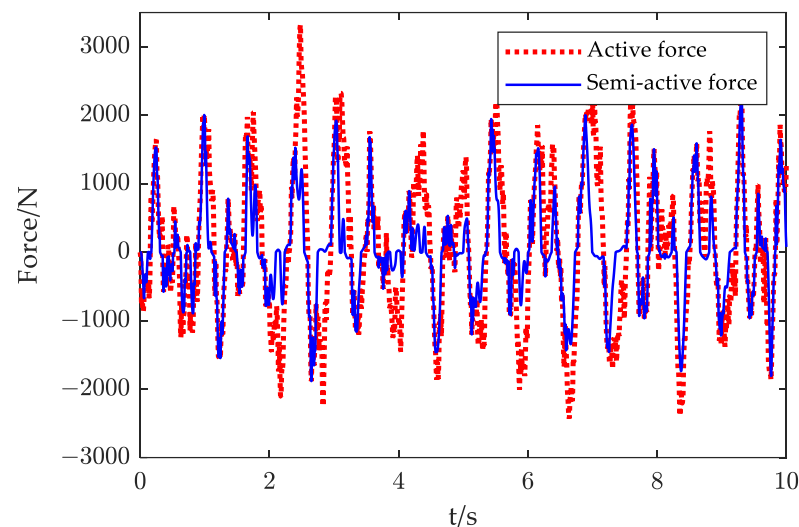

Figure 12. Semi-active force versus active force under random road.
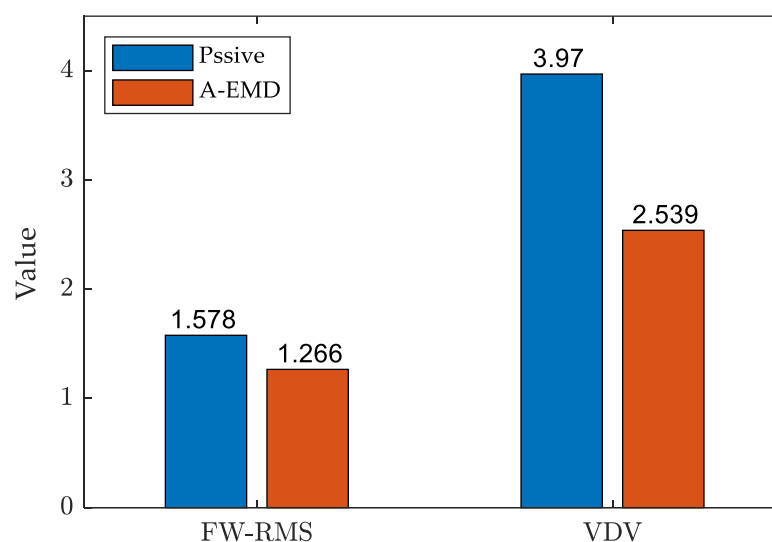

Figure 13. Evaluation parameters.

The simulation method for random road excitation conditions was appropriated to bump road excitation. The bump road responses of the two suspensions are compared in Figure 14, and the PTP values are shown in Table 5.

We can infer from Figure 14a that the performance of suspension is similar to random road in that the cab acceleration is optimized (−22.78%), which can be seen clearly in Table 5. From the human point of view, the VDV acceleration value, which is shown in Figure 13,

also decreases by 36.05%. This could illustrate that A-EMD can effectively reduce the strong impact caused by road surface compared with the passive one. The difference between the results in Figures 11 and 14 is that the car suspension dynamic deflection and tire dynamic load of A-EMD slightly deteriorated compared to the passive suspension. This is due to the harsher road conditions on the bump road, where the controller sacrifices a little vehicle suspension dynamic travel and tire dynamic load performance in order to ensure acceptable ride comfort, i.e., lower cab acceleration. However, despite the deterioration, they did not exceed the limits.
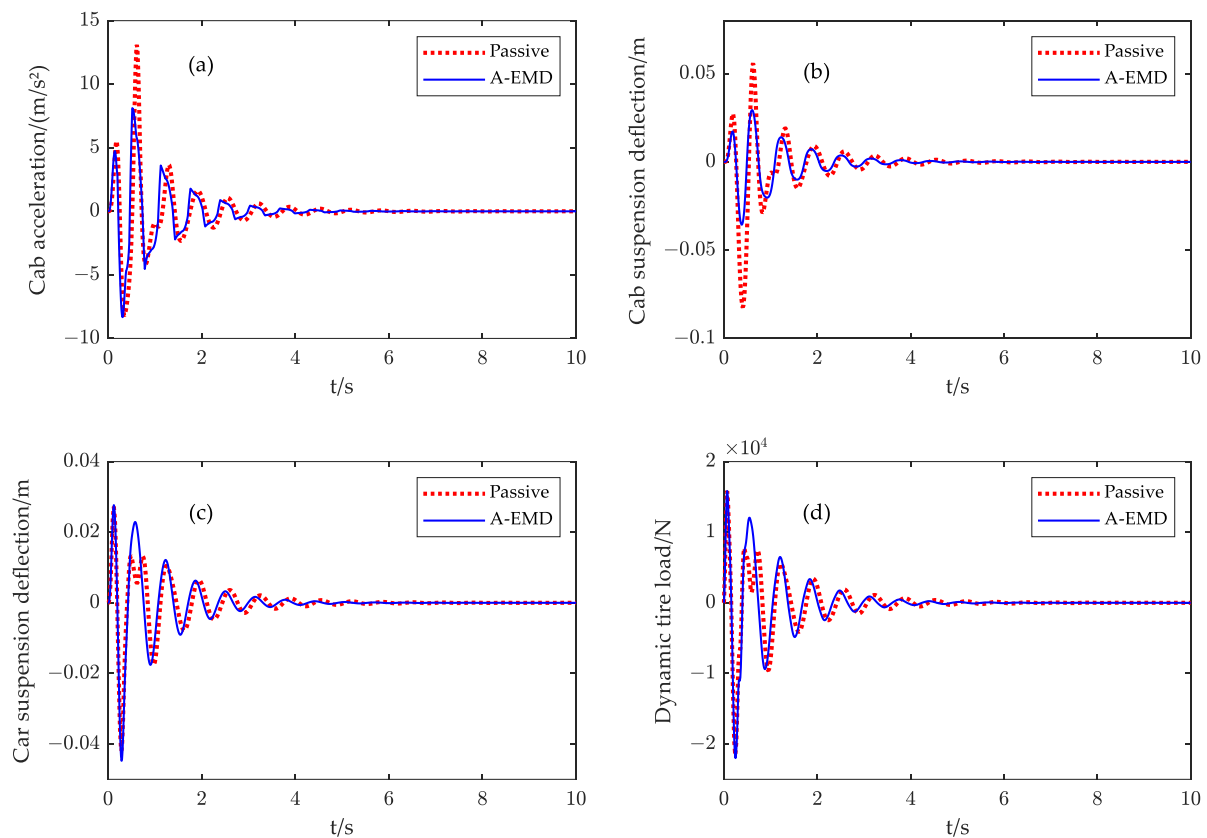
Figure 14. Response under bump road excitation: (**a**) cab acceleration; (**b**) cab suspension deflection; (**c**) car suspension deflection; (**d**) dynamic tire load.

Table 5. PTP values.

Object	Passive	A-EMD
Cab acceleration (m/s^2)	21.3003	16.4479
%	—	−22.78
Cab suspension deflection (m)	0.1382	0.0649
%	—	−52.99
Car suspension deflection (m)	0.0690	0.0724
%	—	4.97
Tire dynamic load (N)	3736.9	3782.7
%	—	1.23

From the above results, we can see that A-EMD has better vibration damping performance than passive suspension on both random and bump roads, and the improvement effects is more than 10%.

5. Conclusions

In this work, a T-S fuzzy modeling approach was adopted to model a quarter-cab car suspension system containing A-EMD, and thereinto, the electromagnetic damper model was verified by the characteristic experiment. Based on the T-S fuzzy model, an H∞ semi-active controller was designed through the PDC method. In addition, a state observer was applied to estimate the suspension system state in real time. Then, numerical simulations were conducted to validate the performance of the designed controller. The results show that the proposed suspension can provide better ride comfort performance than the passive one. The VDV acceleration under bump road and the FW-RMS acceleration under the random road decreased by 36.05% and 19.77%, respectively. In future research, both electromagnetic dampers and air springs could be controlled for the integrated control of damping and stiffness.

Author Contributions: Conceptualization, B.Z. and B.T.; methodology, M.L.; software, M.L.; validation, K.W., J.L. and Y.D.; formal analysis, M.L.; investigation, A.Q.; resources, B.Z.; data curation, Y.D.; writing—original draft preparation, M.L.; writing—review and editing, M.L.; visualization, B.T.; supervision, B.Z.; project administration, B.T.; funding acquisition, B.Z. All authors have read and agreed to the published version of the manuscript.

Data Availability Statement: The data presented in this study are available upon request from the corresponding author.

Conflicts of Interest: The authors declare no conflict of interest.

Nomenclature

m_c	the cab mass	k_i	the torque constant
m_s	the sprung mass	k_e	the voltage constant
m_v	the unsprung mass	r_b	the transmission ratio of the ball screw
k_c	the stiffness of the air spring	R_m	the internal resistance of the generator
k_s	the stiffness of the car suspension	$\widetilde{R}$	the variable resistance
k_t	the tire stiffness	$R_{\max}$	the maximum value of the variable resistance
c_c	the damping of the electromagnetic damper	ω	the generator rotation speed
c_p	the fixed damping of cab suspension	E	the generated voltage
c_s	the damping of the car suspension	I	the current of generator external circuit
z_c	displacement of the cab mass	$\bar{k}_c$	upper bound for the air spring stiffness
z_s	displacement of the sprung mass	$\underset{c}{k}$	upper bound for the air spring stiffness
z_v	displacement of the unsprung mass	h_1, h_2	the fuzzy membership functions
z_r	the road displacement input	$z_{\max 1}$	cab suspension limits travel
u	the force of the electromagnetic damper	$z_{\max 2}$	car suspension limits travel
P_0	the initial pressure of the air spring	γ	the performance index
V_0	the initial volume of the air spring	n_{00}	the cut-off frequency of road space
h_0	the initial height of the air spring	n_0	the standard spatial frequency
P_a	the atmospheric pressure	h_b	the height of the bump
n	the multivariate exponent	l	the length of the bump
A_e	the effective area of the air spring	v_0	the vehicle forward velocity
Δh	the air spring deformation	K_h	the state feedback gain matrices
P	the absolute pressure in the air spring	L_h	the observer matrices gain
V	the volume of the air spring		

References

1. Tan, B.; Zhang, N.; Qi, H.; Zhang, B.; Wang, K.; Liu, J. Nonlinear dynamic analysis and experiments of a pressure self-regulating device for hydraulically interconnected suspension systems. *Nonlinear Dyn.* **2022**, *111*, 4173–4190. [CrossRef]
2. Sim, K.; Lee, H.; Yoon, J.W.; Choi, C.; Hwang, S.-H. Effectiveness evaluation of hydro-pneumatic and semi-active cab suspension for the improvement of ride comfort of agricultural tractors. *J. Terramech.* **2017**, *69*, 23–32. [CrossRef]
3. Tan, B.; Lin, X.; Zhang, B.; Zhang, N.; Qi, H.; Zheng, M. Nonlinear modeling and experimental characterization of hydraulically interconnected suspension with shim pack and gas-oil emulsion. *Mech. Syst. Signal Process.* **2023**, *182*, 109554–109571. [CrossRef]
4. Soliman, A.M.A.; Kaldas, M.M.S. Semi-active suspension systems from research to mass-market–A review. *J. Low Freq. Noise Vib. Act. Control.* **2019**, *40*, 1005–1023. [CrossRef]
5. Ma, R.; Do, C.M. Comfort-oriented Semi-active Matching Design with a Magneto-Rheological Air Suspension Mechanism. *Iran. J. Sci. Technol. Trans. Mech. Eng.* **2020**, *45*, 699–709. [CrossRef]
6. Weber, F.; Spensberger, S.; Obholzer, F.; Distl, J.; Braun, C. Semi-Active Cable Damping to Compensate for Damping Losses Due to Reduced Cable Motion Close to Cable Anchor. *Appl. Sci.* **2022**, *12*, 1909–1926. [CrossRef]
7. Yan, S.; Gu, Z.; Park, J.H.; Xie, X. Adaptive memory-event-triggered static output control of T–S fuzzy wind turbine systems. *IEEE Trans. Fuzzy Syst.* **2022**, *30*, 3894–3904. [CrossRef]
8. Yan, S.; Gu, Z.; Park, J.H.; Xie, X. Sampled Memory-Event-Triggered Fuzzy Load Frequency Control for Wind Power Systems Subject to Outliers and Transmission Delays. *IEEE Trans. Cybern.* **2022**, 1–11. [CrossRef]
9. Yan, S.; Gu, Z.; Park, J.H.; Xie, X. Distributed-Delay-Dependent Stabilization for Networked Interval Type-2 Fuzzy Systems With Stochastic Delay and Actuator Saturation. *IEEE Trans. Syst. Man Cybern. Syst.* **2022**, 1–11. [CrossRef]
10. Güvenc, B.A.; Kural, E.; Keşli, B.; Gülbudak, K.; Güngor, S.; Kanbolat, A. Semi Active Suspension Control System Development for a Light Commercial Vehicle. *IFAC Proc. Vol.* **2006**, *39*, 391–396. [CrossRef]
11. Qin, Y.; Zhao, F.; Wang, Z.; Gu, L.; Dong, M. Comprehensive Analysis for Influence of Controllable Damper Time Delay on Semi-Active Suspension Control Strategies. *J. Vib. Acoust.* **2017**, *139*, 031006. [CrossRef]
12. Sun, S.; Tang, X.; Yang, J.; Ning, D.; Du, H.; Zhang, S.; Li, W. A New Generation of Magnetorheological Vehicle Suspension System With Tunable Stiffness and Damping Characteristics. *IEEE Trans. Ind. Inform.* **2019**, *15*, 4696–4708. [CrossRef]
13. Yao, G.Z.; Yep, F.F.; Chen, G.; Li, W.H.; Yeo, S.H. MR damper and its application for semi-active control of vehicle suspension system. *Mechatronics* **2002**, *12*, 963–973. [CrossRef]
14. Guo, D.L.; Hu, H.Y.; Yi, J.Q. Neural Network Control for a Semi-Active Vehicle Suspension with a Magnetorheological Damper. *J. Vib. Control* **2004**, *10*, 461–471. [CrossRef]
15. Tang, X.; Du, H.; Sun, S.; Ning, D.; Xing, Z.; Li, W. Takagi–Sugeno Fuzzy Control for Semi-Active Vehicle Suspension With a Magnetorheological Damper and Experimental Validation. *IEEE/ASME Trans. Mechatron.* **2017**, *22*, 291–300. [CrossRef]
16. Ning, D.; Du, H.; Sun, S.; Li, W.; Li, W. An Energy Saving Variable Damping Seat Suspension System With Regeneration Capability. *IEEE Trans. Ind. Electron.* **2018**, *65*, 8080–8091. [CrossRef]
17. Wang, D. Study on Height Control of a Bus Equipped with HIS System and ECAS System. Master's Thesis, Hunan University, Hunan, China, 2018.
18. Marzbanrad, J.; Zahabi, N. H∞ active control of a vehicle suspension system exited by harmonic and random roads. *Mech. Mech. Eng.* **2017**, *21*, 171–180.
19. Du, H.; Li, W.; Zhang, N. Integrated Seat and Suspension Control for a Quarter Car With Driver Model. *IEEE Trans. Veh. Technol.* **2012**, *61*, 3893–3908.
20. Xia, X. Research on Vibration Control Algorithm of Seat Suspension Based on an Energy Saving Continually Controllable Electromagnetic Variable Damping System. Master's Thesis, Hefei University of Technology, Anhui, China, 2020.
21. Lo, J.C.; Lin, M.L. Observer-based robust H∞ control for fuzzy systems using two-step procedure. *IEEE Trans. Fuzzy Syst.* **2004**, *12*, 350–359. [CrossRef]
22. Zhang, B.; Tan, C.A.; Dai, T. Ride comfort and energy dissipation of vehicle suspension system under non-stationary random road excitation. *J. Sound Vib.* **2021**, *511*, 116347–116364. [CrossRef]
23. Du, H.; Lam, J.; Cheung, K.C.; Li, W.; Zhang, N. Direct voltage control of magnetorheological damper for vehicle suspensions. *Smart Mater. Struct.* **2013**, *22*, 105016–105029. [CrossRef]